

Developing a Pipeline for Statistical Shape Modelling of Intracranial Arteries in Stroke Patients Using Clinical CTA Imaging: A comprehensive analysis of vascular geometry and variability

Noah Saad (5222117), Ruben Terwint (5362679), Luuk van Weelden (5076935), Ole Visser (4964322)

Abstract—This paper showcases the results of a Statistical Shape Model (SSM) pipeline used to describe the variation of the intracranial arteries (IAs) between different samples as well as a refined method of converting and cleaning brain CTA's scans to usable 3D models of the intracranial arteries. The validation of this pipeline was successfully done on different geometries such as hip geometries, aorta and pelvis geometries. However, due to the high complexity and variability of the intracranial arteries, a division into smaller segments was necessary for the analysis as opposed to using the whole structure.

I. INTRODUCTION

Currently, stroke is the second leading cause of death. According to the World Health organisation fact-sheet released in 2022, the "lifetime risk of developing a stroke has increased by 50% in the last 17 years and now 1 in 4 people is estimated to have a stroke in their lifetime" [1].

The cerebrovascular system plays a crucial role in all facets of this disease, however research into the morphological components of this system is relatively scarce. The goal of this project is to: firstly build a framework that creates 3D models of the main intracranial arteries (IAs), more specifically the ones forming Circle of Willis (CoW), seen in figure 1 from Computed Tomography Angiography (CTA) scans of patients; and secondly, to use Statistical Shape Modelling to compare this vasculature shape among stroke patients and be able to create an average/global shape that best describes these patients' intracranial arteries. Furthermore, we are also interested in the different modes that describe how the vessels differ from the mean shape. This will hopefully enable the health specialists to overcome the great variability of this specific vasculature and to be able to better prepare for stroke patient treatment as they need immediate attention to increase their chances at survival.

For many years the CoW was believed to be a "compensatory system in the case of arterial occlusion" [2]. However, research has started discussion about this idea and it has showed that the CoW most likely has a blood pressure levelling function due to its many different curved branching arteries and more progressive branching to arterioles that provide additional resistance and thus provide protection from the high stresses that occur on the arterial walls. This is due to the pulse wave produced by the heart which induces highly variable pressures on the Blood to Brain Barrier.

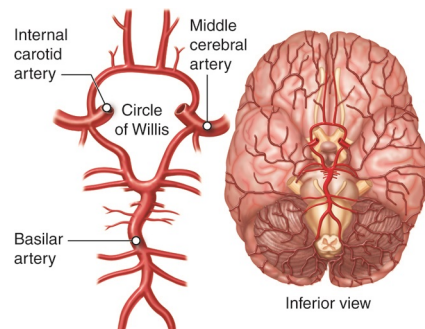


Figure 1: A schematic figure of the Circle of Willis [3]

There has already been research into the variability of the intracranial vasculature, more specifically the circle of Willis. An estimated $68.22 \pm 14.32\%$ of the human population has an anatomical variation in the circle of Willis alone. It has also been found that there are, in total, 82 possible variations of the CoW due to the fact that arteries can be missing or hypoplastic (underdeveloped) as can be seen in figure 2 [4].

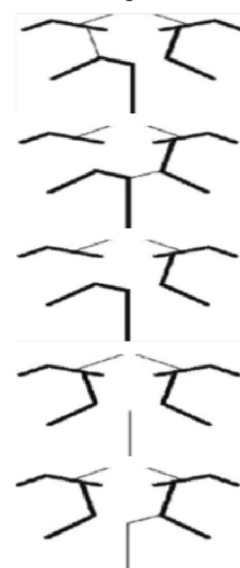


Figure 2: Different possible CoW geometries [4]

This greatly increases the difficulty of treating this area which lies at the base of the skull and is an important

risk factor for the development of strokes. Studies have also shown that stroke patients are more likely to have a variant in their CoW. More than half of the times these are located in the posterior part of the CoW [5]. This reinforces the idea that the variability of this geometry has to be investigated further in the stroke patient group to improve our understanding and in turn be able to better treat stroke patients. This leads us to our research question.

RESEARCH QUESTION AND HYPOTHESIS

How does the shape of the intracranial vasculature vary in a given sample of ischemic stroke patients, with an emphasis on the intracranial arteries and Circle of Willis?

This research attempts to discover how anterior and posterior variant types of the CoW are connected, as well as the variation in prominent surrounding arteries.

There is, however, earlier research into the variability of the CoW which views the two variant types as separate occurrences. Therefore, the hypothesis is that the percentage of found anomalies should approximately match that of "Variants of the circle of Willis in ischemic stroke patients" [5], which analyses a sample group of similar size.

This research has been conducted as part of the Bachelor End Project for Mechanical Engineering students at the TU Delft.

II. THEORY

In recent years, the medical field has taken to Statistical Shape Modeling (SSM) as a means of analysing model variations. Usually used on organs such as bones or livers, SSM maps the variability in a group of shapes and can then be used for tasks such as classification, segmentation, and generation of new shapes. This is the method that this research intends to use.

In this section we will explore how the SSM performs its analysis. Firstly, the dataset is a collection of shapes described by a mesh, let each shape's mesh be represented by a shape vector $V = [v_1, v_2, v_3, \dots, v_{n_m}]^T$, where n_m is the number of nodes. Let n_s be the number of shapes in the dataset. The first thing needed for the analysis is the mean shape which is obtained by summing every object's shape vector and dividing by the number of samples:

$$\bar{V} = \frac{1}{n_s} \sum_{i=1}^{n_s} V_i \quad (1)$$

After the mean shape is obtained, the covariance matrix is computed to determine the covariance between shape variations across the dataset using the following equation:

$$\Sigma = \frac{1}{n_s} \sum_{i=1}^{n_s} (V_i - \bar{V})^T (V_i - \bar{V}) \quad (2)$$

Now that the covariance matrix has been obtained, the following step is to apply Principal Component Analysis (PCA) (a dimensionality reduction method) to the covariance matrix to identify the principal components of shape variation in the dataset. From basic linear algebra, the eigendecomposition of Σ , seen in eq. 3, gives us the principal components (eigenvectors) and their associated weights (eigenvalues), which represent the magnitude of the variation across their eigenvectors. These can describe the variation of the shape in the set, where m_i are the modes of the model and λ_i their associated weight [6]. Ideally, one is left with n modes where $n < n_s$ as then a finite number of modes can be used to describe an infinite number of different vasculatures.

$$\Sigma = [m_1 \dots m_{n_s}] \begin{bmatrix} \lambda_1 & & \\ & \ddots & \\ & & \lambda_{n_s} \end{bmatrix} [m_1 \dots m_{n_s}]^T \quad (3)$$

III. METHODS

A. CTA scan to 3D model

After receiving the CTA files from the Erasmus Stroke Study database, 3D models of the CoW could be created. The process to obtain the models had a few steps. First, the CTA files were imported into the programme '3D Slicer' [7]. Here, all relevant vessels were identified and selected. This was done by firstly applying a grey-scale threshold to the CT scan. With this threshold most important vessels were identified, but a lot of bone was also selected. To help isolate the vessels from surrounding bone, the 'grow seeds' function present in 3D slicer was exploited, in which vessels and bones are manually marked (as vessel and bone respectively) throughout several layers of the CT scan. In this way it was possible to make a more accurate 3D model of the vasculature.

The models now looked like Figure 3 Left below, with most important arteries included, but, as seen, also lots of insignificant vessels and bone material. Therefore, the final step of the processing was discarding the areas of no interest. This was done by exporting the 3D model from 3D Slicer into Meshmixer [8] for further improvement. Here a series of 'plane cuts' were used to discard certain vessels and the 'sculpt' tool was used to get rid of bone. However, the sculpt tool was imperfect and left very thin lines sticking out of the vessels. Visually these were almost unnoticeable but created problems in further steps, so had to be carefully removed. Afterwards the models were exported and saved in a database, ready to be used for SSM. An example of a final product can be seen in Figure 3 Right.

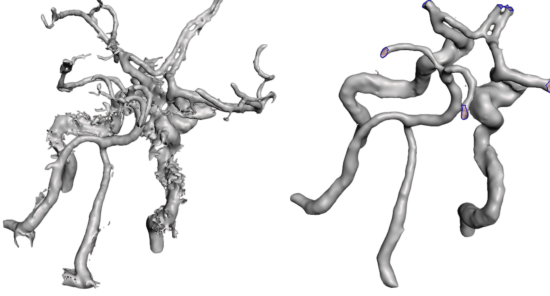


Figure 3: Left: STL file of the CoW and relevant vessels after using 3D slicer. Right: Final STL file of the IAs after processing in Mesh Mixer.

B. Preprocessing of STL files prior to SSM

1) *Remeshing*: The models obtained after the post processing in Meshmixer had an excessive amount of nodes and triangles. It was decided to remesh the object such that the total number of nodes is greatly reduced while still having enough nodes to accurately describe the shape of the object. This step was completed using the software ShapeWorks [9].

2) *Generating Landmarks*: It is crucial that the alignment of the nodes of the models are correct. If that is not the case, the SSM will generate inaccurate results. As such, it was decided to create an algorithm that could accurately align objects.

Prior to the algorithm, it is first noteworthy to discuss what exactly will align. It may be tempting to align the nodes of the mesh file of each CoW as that is generated automatically. However, two files rarely have the same number of nodes. If the number of nodes are not the same, it would be incorrect to compare these two objects. As a reminder, the SSM is generated using the Principal Component Analysis. Using the theory established in section II, if v_{n_m} is different for each shape, one cannot compare these objects with each other. Hence it is necessary to have an algorithm that generates "landmarks" on each shape such that all shapes have the exact same number of landmarks. Furthermore, the landmarks need to be generated with respect to the nodes of the mesh, such that they are an accurate representation of the shape.

To generate the landmarks, there are a few common clustering algorithms that can be utilised, namely the K-means method and the Gaussian Mixture Model (GMM) from the Scikit-learn module in Python [10].

The landmarks generated using the K-means method did not differ much compared to the ones generated using the GMM as can be seen in figure 4 (a model of a femur was used for simplicity). As there is not much difference, the K-means method was utilised as it converged on average faster.

Additionally, the number of landmarks also needed to be decided. A number of clusters was assigned and then landmarks were generated. The sum squared error (SSE) of each node to the landmark is calculated as well as the silhouette coefficient to determine what is the optimal number of landmarks to accurately describe the geometry. The silhouette coefficient is computed using the average within-cluster distance (a) and the average distance to the nearest cluster (b)

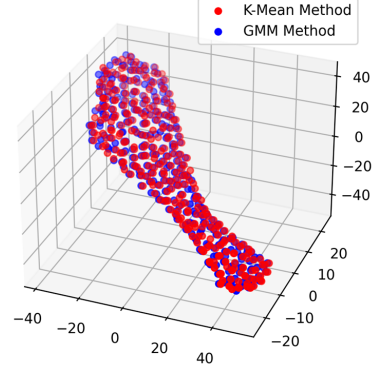


Figure 4: Landmarks generated from K-means (red) and from Gaussian Mixture Model (GMM) (blue) on a femur.

for each sample. The sample silhouette coefficient is $\frac{(b-a)}{\max(a,b)}$. For clarity, b is the distance between the sample and the closest cluster to which it does not belong. A summary of the findings are in Figures 5 and 6 where a geometry of the IAs was evaluated. The total number of landmarks that was used was 3200 landmarks. This ensured almost no error and a silhouette coefficient of over 90%.

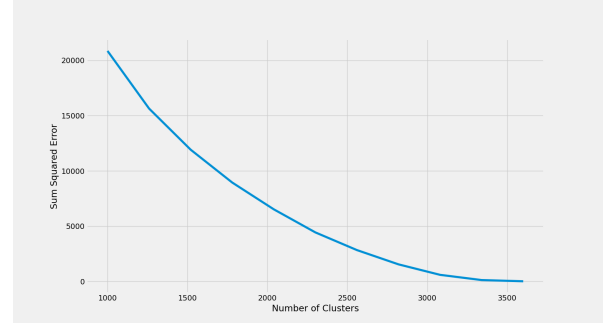


Figure 5: Sum Squared Error for different number of clusters/landmarks

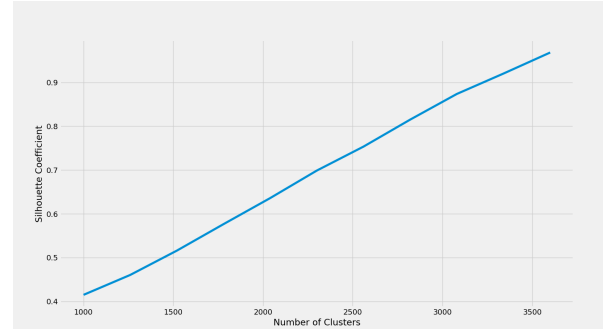


Figure 6: Silhouette coefficient for different number of clusters/landmarks

3) *Correspondence and Alignment*: As a result of the K-means clustering, each objects' points are represented in a 3D array, where each row is a landmark. As the clusters are

generated randomly, the landmarks' place in the matrix is random, and therefore, when comparing two matrices row by row, one must ensure that each row represents a specific location. For example, the first row for each object list should represent the top left of the object. Here it is useful to choose a reference geometry where all other geometries will be aligned to. This is a classic assignment problem and it has been researched thoroughly. From the literature, a solution to this is the Hungarian Algorithm [11].

Equation 4 minimises the cost and solves the problem where each $C_{i,j}$ is the cost of matching vertex i of the first partite set (a "worker") and vertex j of the second set (a "job"), and let X be formally described as a boolean matrix where $X_{i,j} = 1$ iff row i is assigned to column j [11]. Then the optimal assignment has cost:

$$\min \sum_i \sum_j C_{i,j} X_{i,j} \quad (4)$$

The relevance for this project is the following. Let the workers be replaced by the points of the reference object and the jobs by the points of the object we would like to create correspondence. The euclidean distance between the reference points and the other points will be the parameter to optimise. As such our matrix is now one which represents the distance of each point with each reference point. By applying the built-in function we can generate a matrix where all rows of all object are representative of the same approximate location. This also disables multiple points to be assigned to the same geographical location, which would be the case if the common Iterative Closest Point (ICP) method was used. Figure 7 shows the effect of non-uniqueness when attempting correspondence between geometries using the Hungarian algorithm and ICP.

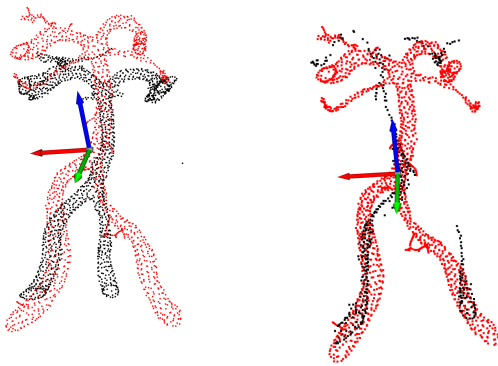


Figure 7: Effect of non-uniqueness on correspondence. On the left, the black geometry is referenced to the red geometry using the Hungarian algorithm, while on the right, Iterative Closest Point (ICP) is used.

Now that landmarks are obtained and are correctly ordered with respect to the reference, a transformation needs to be found for each object such that they are aligned with each other. This is also known as Procrustes alignment. However,

the alignment will not include the scaling of the data. Due to the nature of the project, the size of the vasculature is also worthy to investigate.

A method to achieve this is by utilising the Singular Value Decomposition (SVD) method on the cross covariance matrix of the two objects. The SVD of the cross covariance matrix outputs three matrices, two rotation/reflection matrices and one scaling matrix. Using the rotation matrices, we can transform the object such that it is aligned with the other. If we wish to do this for all our files, it is useful to select a reference geometry to which we will compare everything to. The effect of the alignment can be seen in figure 8.

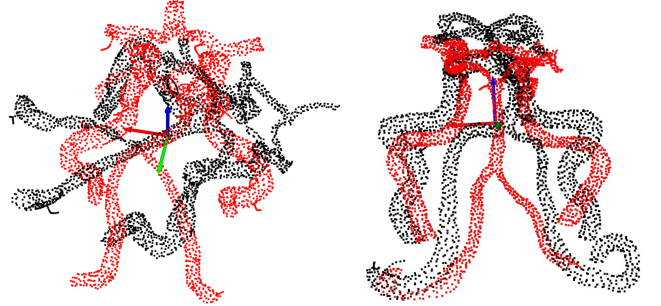


Figure 8: Left: Two shapes prior to alignment. Right: After alignment. Reference object (red) and object to-be-aligned (black)

C. Statistical Shape Model

Using the formulas introduced in section II, the mean shape can be calculated as well as the eigenvectors and eigenvalues representing the modes and their weights respectively.

IV. VALIDATION OF METHODOLOGY

In order to validate the method, different data sets were utilised, encompassing a range of anatomical structures. These data sets included geometries of the right hip [12] and the aorta [13]. By incorporating diverse anatomical shapes, the method was rigorously tested and evaluated across various scenarios. The inclusion of the right hip geometry enabled the assessment of the method's performance and accuracy specifically in relation to this joint. The femur geometry data set validated the robustness and applicability of the method to a major bone structure, while the aorta geometry data set facilitated the examination of its effectiveness in a vascular context. The aorta files originated from a synthetic sample generated using Statistical Shape modelling. As such by applying our method, one should be able to achieve similar means and modes as the paper by Romero et. al. [13].

A. Data Set of Right Hip

Figure 9 shows the result of the SSM on the right hip. Figure 10 displays the cumulative variance of each mode in the model. Furthermore, in order to validate our model, it was tested in trying to reconstruct a shape that was used to construct the model as well as a new shape. This was to ensure firstly that the SSM truly worked and also to evaluate how

well the model can describe new shapes. This can be seen in Figures 11 and 12, where only the first three modes were used for reconstruction and where the model tries to reconstruct an unseen shape. The figures show that the model can effectively describe the shape of an unseen figure, reconstructing it perfectly. As such the model can be deemed correct.

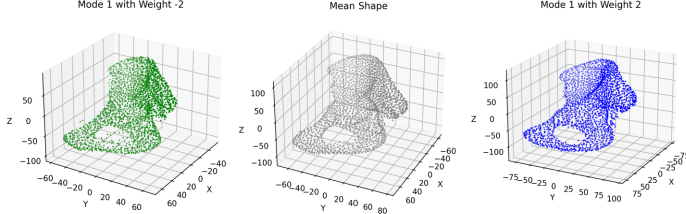


Figure 9: Statistical Shape Model results for right hip dataset. Left: Mean Shape morphed with the first mode and weight -2 times the standard deviation. Middle: Mean Shape. Right: Mean Shape morphed with the first mode and weight 2 times the standard deviation

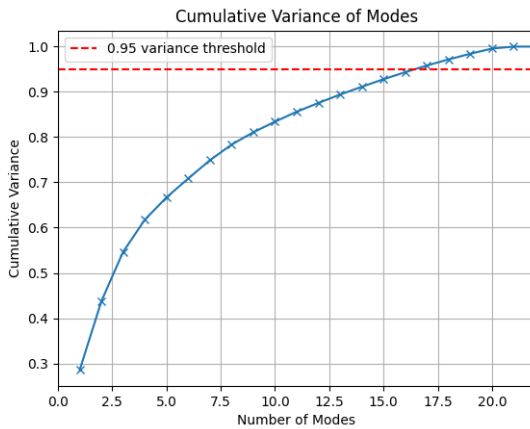


Figure 10: Cumulative variance of the modes of the model. To obtain 95% cumulative variance, 16 modes are required.

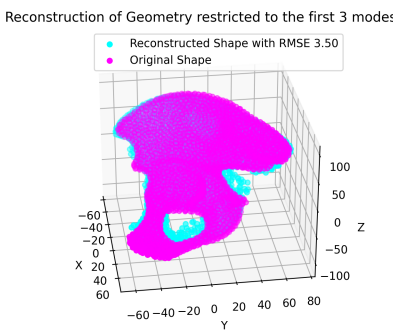


Figure 12: Reconstruction of Hip for unseen geometry without restriction for modes

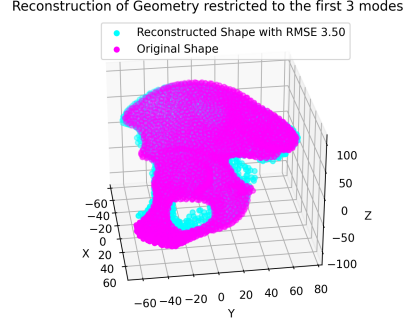


Figure 11: Reconstruction of Hip. Up: Restriction to first three modes

B. Data Set of the Aorta

The same method was applied to a set of 81 geometries of the aorta. The model underwent the same testing to ensure its validity (mean shape with modes, cumulative variance plot, and reconstruction attempt with and without restriction on seen and unseen geometry respectively). These results can be seen in Figures 13 and 14.

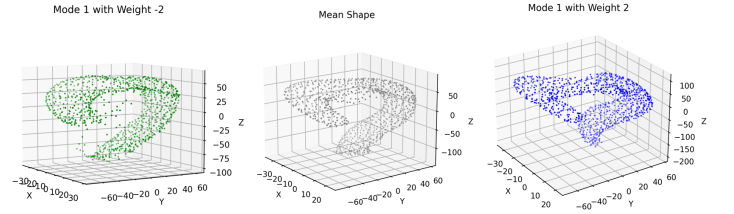


Figure 13: Statistical Shape Model results for right hip dataset. Left: Mean Shape morphed with the first mode and weight -2 times the standard deviation. Middle: Mean Shape. Right: Mean Shape morphed with the first mode and weight 2 times the standard deviation

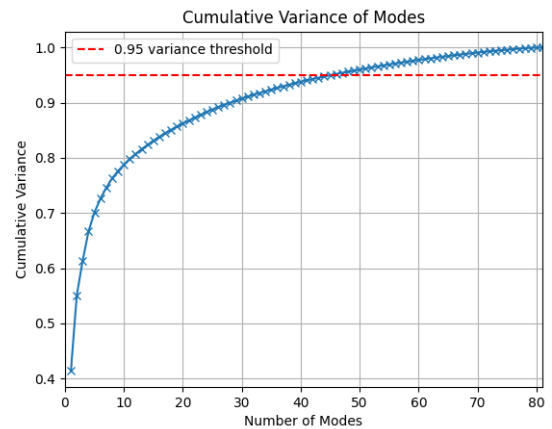


Figure 14: Cumulative variance of the modes of the model. To obtain 95% cumulative variance, 45 modes are required.

As the model performed well for both the hip and the aorta, we are confident that the method is valid and can be used to meet the goal of the paper.

C. Testing on Complete Intracranial Arteries

While applying the method on the complete geometry, the SSM yielded disappointing results. The average shape can be seen in Figure 15. Too much information is lost due to severe variability in the geometries. While the methodology explained above ensures correspondence and alignment, the geometries are too different for SSM to yield a decent result. An important criterion that is required for all geometries in the training set is that they are anatomically the same, that is they contain the same arteries and these arteries must be cut at the same location for each subject. Due to the variability of the vessels in this region as explained in section I, it was a complex task to achieve sufficient geometries that met that standard.

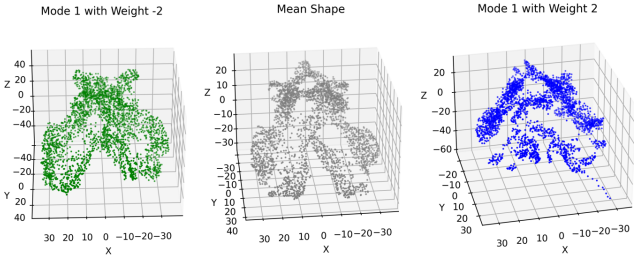


Figure 15: SSM on the complete geometry. Left: first mode with weight -2 times the standard deviation. Middle: Mean Shape. Right: first mode with weight 2 times the standard deviation.

As such, it was decided to run the SSM on individual arteries instead of the geometry as a whole. The separation of the complete geometry into the different components can be seen in Figure 16.

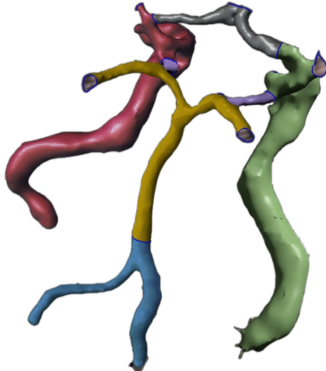


Figure 16: Separation of the complete intracranial arteries for SSM

V. RESULTS

The SSM was run on all the separate segments of the IAs. The results are displayed below. At first the mean shape is shown next to the first mode with weight -2 standard deviation and 2 standard deviations. Due to the limited number of geometries the modes look rather extreme. Figures 17 and 18 is the result of the SSM on the IAs. Furthermore, the results only display the four segments that are most relevant in a clinical setting. These are the two ICAs as well as the vertebral arteries and the basilar and the posterior cerebral arteries. As an example, a study conducted by Chen et. al. [14] as well as a study conducted by Bartstra et. al. [15], most of the calcification is found in these regions and as such, it can be more of interest to model these sections. The SSM was also run on the other portion of the geometry however, this region is less clinically relevant.

It is to be noted that all the point clouds of the same object in the results share the same number of landmarks. As such, when for example the diameter of a vessel appears larger, such as in the mean shape of Figure 18d, it does not mean that there is a gap in the geometry, but rather that the vessel is larger. All landmarks are representative of the surface of the object. If a reconstruction of the surface were to be conducted, one could veritably see the completeness of the vessel without the apparent gap.

The first mode for all shapes relate to the change in diameter of the geometries. Due to the limited geometries, the change seems extreme. Other modes for these vessels can be found in the appendix in sections B through E.

Furthermore, a ptest was also utilised on a shape in the data set to validate which modes are statistically most likely to contribute to changing the mean shape to best match it. These results can be found in the appendix in section F

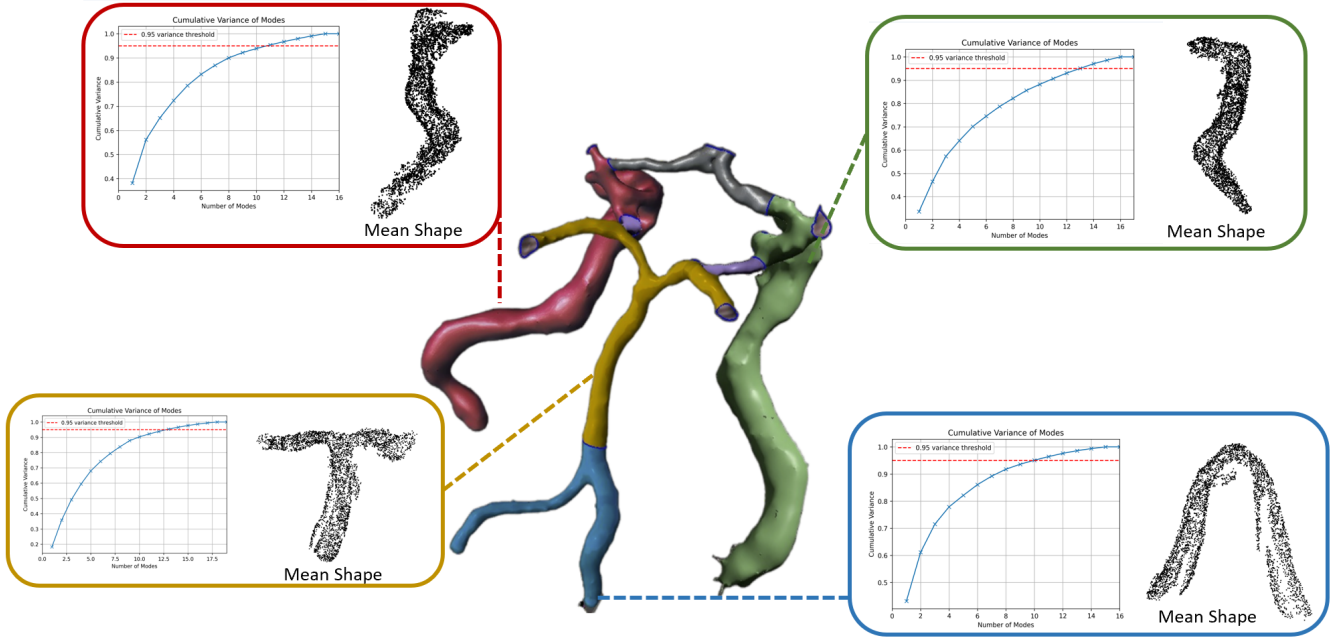
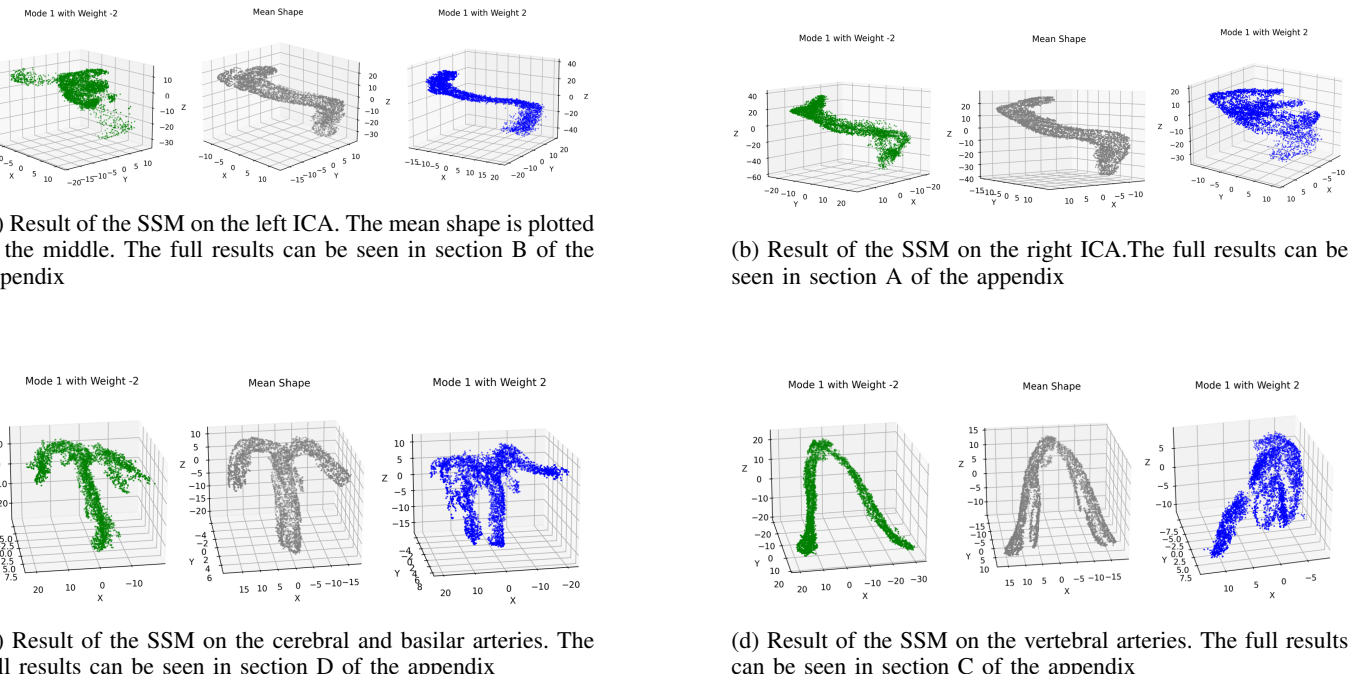


Figure 17: Average geometry and cumulative variance plots of the left ICA (red), right ICA (green), the basilar and posterior cerebral arteries (yellow) and the vertebral arteries. The mean shape is represented as a point cloud. A cumulative variance plot is also given. A 95% desired threshold is chosen.



(c) Result of the SSM on the cerebral and basilar arteries. The full results can be seen in section D of the appendix

(d) Result of the SSM on the vertebral arteries. The full results can be seen in section C of the appendix

Figure 18: Modes plotted for each region of interest: Left ICA 18a, Right ICA 18b, cerebral and basilar arteries 18c, vertebral arteries 18d. Plotted left is the first mode with weight -2 standard deviations. Plotted right is the first mode with weight 2 standard deviations. The mean shape is plotted in the middle.

VI. DISCUSSIONS

A. Limitations

The pipeline created for SSM, faced no real issues. The limitation was the number of files we could feed our model. This was due to issues with converting CTA-scans to functional STL files, which will be described in this sub-chapter.

To start, the programme given (to convert CT-scans to STL) was 3D Slicer, which has very limited automation possibilities which meant that all segmentation had to be done manually.

Furthermore, 3D Slicer worked less than optimal. As described in section III, a combination of grey-scale thresholds and the 'grow seeds' function is used to distinguish arteries from bone. This, however, resulted in poorer results than expected, partly due the old age and thus low resolution of the scans (the scans were collected between 2005 and 2010). 3D-slicer could not isolate the arteries entirely and therefore a lot of bone was still 'attached' to the blood vessels, as shown in Figure 19. This could not be helped; when changing the threshold to erase bone, valuable information about important arteries would be lost and growing more seeds was not very effective.

So the bone had to be trimmed in Meshmixer, which was a slow process. Especially the removal of the thin lines that remained after using the 'sculpt' tool took a long time.

In Meshmixer it also became apparent that a lot of the STL's made in 3D Slicer were not useful (due to missing parts that were first hidden in bone or non-connected vessels) and thus had to be discarded.

To summarise, 3D-slicer was less effective than first thought which meant we had to discard STL's last-minute and caused the time needed to post process with Meshmixer to increase significantly. This could not be compensated by automation of steps. In the end we converted 41 CTA-scans to STL's, but after filtering and preprocessing only 19 were useful for our SSM.

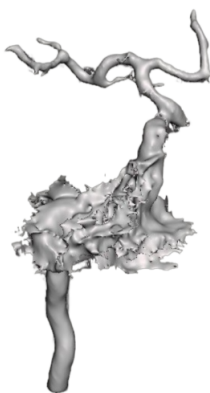


Figure 19: Bone material attached to the blood vessels in STL.

B. Circle of Willis and other Extremes

In our research question we mentioned the desired emphasis on the Circle of Willis. This has not been possible. As mentioned before, 3D-slicer proved less effective than desired.

This translated in an inability to identify smaller arteries like those in the CoW without covering the nearly all the vessels in bone. Eventually less than 20% of the created STL's had a Posterior Communicating Artery (a vessel in the Circle of Willis, abbreviated as PCom). Showing that the STL's are not fully representative of the research group [16].

For SSM to work the vessels have to be anatomically similar, meaning that STL's with certain parts of the CoW cannot be compared to those lacking those parts. So the ones with PComs were divided from the ones without. Unfortunately, there were so little functional STL's with PComs that running SSM on them, as a set, would not yield useful results. Therefore, we were not able to emphasise the Circle of Willis in our research.

Likewise, we had to eliminate other extreme variations of vessels as they were not anatomically similar, for example a Vertebral Artery with a bifurcation.

C. Homogeneous vs Entropy-based Landmarks

In this research Kmeans was used for homogeneous landmark placement. This distributes randomly and works well for shapes that are relatively similar. For shape sets like the hip and aorta, this works perfectly, as well as for the set of vertebral arteries (blue in Figure 16) and the set of basilar and posterior cerebral arteries (yellow in Figure 16).

However, the ICA's differ a lot in terms of absolute displacements and difference in curvature as such a random distribution does not work as well in these circumstances. The problem occurs in alignment, the randomness of landmark in combination with the extreme displacements causes issues in the SSM. Experimenting with a entropy-based, heterogeneous landmark placement from ShapeWorks [9], the result was a better landmark correspondence and thus a better mean shape when dealing with large variability.

VII. CONCLUSION

A. Summary

In examining the shape of the intracranial vasculature in a sample of ischemic stroke patients, with a particular focus on the intracranial arteries and Circle of Willis, its variability has been captured using Statistical Shape Models (SSM).

The intracranial arteries were divided into five different segments for better results. Of those five segments, the mean shape was found as well as modes that are able to describe any individual artery.

B. Recommendations for Future Research

In this research a strong pipeline for SSM is created, the main component missing is data. Even though there were over a thousand CTA-scans available, there were roughly only twenty functional STL's made. The reasons for this are mentioned in the discussion, but the primary reason was that the CT-scans had to be manually converted to STL. Therefore the main recommendation for future research is to automatise the steps described in subsection III-A. In this way more of the data can be fed to the SSM and the results

drastically ameliorate. With enough functional data, extreme variations could also be divided into their own categories (either manually or automatically) and have their own SSM.

A method for automating the process can be using the DeepSSM (a deep learning framework) which can augment the data set using machine learning [17]. Furthermore, if enough segmentations are made, a convolutional neural network could be trained to automate going from a CTA to a 3D model, however a lot of training data is required for good results.

Another recommendation is, if possible, to use newer CT-scans. The CT-scans used in this research were around 15 years old and often had a poor resolution. In the time since, technology has made great progress and scans are now much clearer. With clearer scans it is more likely for a programme such as 3D Slicer to pick up on smaller arteries. Once there is an effective way to identify these vessels, the Circle of Willis and its variations can be properly investigated which was the original emphasis of this research.

As of now, the mean shapes and modes are represented by point clouds. It would be helpful for computational research if these clouds could also be converted to STL files. Implementing this using solely point clouds is impossible as there needs to be information on the connectivity of the landmarks. Should such information be included, the SSM could yield better results and generating an STL file representing the mean shape as well as how it changes could be viable. Furthermore, using the information about the connectivity of the points can also result in the modes being less extreme and unrealistic.

Using Kmeans creates a homogeneous spread of landmarks, see subsection III-B2. This method works well for geometries that resemble each other or rather that are not extremely different to each other. For geometries where that is not the case, the aforementioned may not always result in desirable outcomes. This is as a result of the correspondence algorithm that may sometimes not work perfectly for highly different geometries. For instance, the ICAs have a large variation in shape within the population. The curvature can vary greatly and misalignment is likely to happen between a geometry that varies greatly from the reference. Both algorithms have their pros and cons, the entropy-based algorithm does not work on geometries that are disconnected, which can be problematic for the complete geometry of the IAs as in some cases the anterior and the posterior portion of the IAs can be disconnected (due to certain variations in the COW).

ACKNOWLEDGEMENTS

We would like to express our sincere gratitude to the following individuals and organisations for their contributions and support throughout the course of this project.

We would firstly like to thank TU Delft for having offered this research as a Bachelor End Project. We are also grateful to Erasmus MC for providing the necessary facilities and resources that were and still are instrumental in the success of this research. We would like to thank our supervisors, Dr.ir. A.C. Ali Akyildiz, Dr. Selene Pirola, Drs. Brian Berghout, M.D. and Drs. Frederica Fontana, for their guidance, expertise, and constant encouragement throughout the research process. Their valuable insights and feedback significantly contributed to the development and refinement of our methodology. They are also the ones responsible for making this project a possibility. Lastly, we are indebted to all the patients that graciously shared their scans to enable this research. Their willingness to take part in the study provided the necessary data for our analysis, and without their cooperation, this project would not have been possible.

REFERENCES

- [1] "World stroke day 2022," Oct 2022.
- [2] Z. Vrselja, H. Brkic, S. Mrdenovic, R. Radic, and G. Curic, "Function of circle of willis," 2014. PMID: 24473483.
- [3] L. U. M. Center, "Drawing circle of willis," *AnatomyTOOL*.
- [4] J. R. Ayre, P. J. Bazira, M. Abumattar, H. N. Makwana, and K. A. Sanders, "A new classification system for the anatomical variations of the human circle of willis: A systematic review," *Journal of Anatomy*, vol. 240, no. 6, pp. 1187–1204, 2022.
- [5] J. De Caro, A. Ciacciarelli, A. Tessitore, O. Buonomo, A. Calzoni, I. Francalanza, C. Dell'Aera, D. Cosenza, C. T. Currò, F. Granata, and et al., "Variants of the circle of willis in ischemic stroke patients - journal of neurology," Mar 2021.
- [6] M. B. Stegmann and D. D. Gomez, "A brief introduction to statistical shape analysis," 2002. Informatics and Mathematical Modelling, Technical University of Denmark, DTU.
- [7] A. Fedorov, R. Beichel, J. Kalpathy-Cramer, J. Finet, J.-C. Fillion-Robin, S. Pujol, C. Bauer, D. Jennings, F. Fennessy, M. Sonka, J. Buatti, S. Aylward, J. V. Miller, S. Pieper, and R. Kikinis, "3d slicer as an image computing platform for the quantitative imaging network," *Magnetic Resonance Imaging*, vol. 30, pp. 1323–1341, Nov. 2012.
- [8] "Autodesk meshmixer."
- [9] J. Cates, S. Elhabian, and R. Whitaker, "Shapeworks: particle-based shape correspondence and visualization software," in *Statistical Shape and Deformation Analysis*, pp. 257–298, Elsevier, 2017.
- [10] F. Pedregosa, G. Varoquaux, A. Gramfort, V. Michel, B. Thirion, O. Grisel, M. Blondel, P. Prettenhofer, R. Weiss, V. Dubourg, J. Vanderplas, A. Passos, D. Cournapeau, M. Brucher, M. Perrot, and E. Duchesnay, "Scikit-learn: Machine learning in Python," *Journal of Machine Learning Research*, vol. 12, pp. 2825–2830, 2011.
- [11] H. W. Kuhn, "The hungarian method for the assignment problem," *Naval Research Logistics Quarterly*, vol. 2, pp. 83–97, Mar. 1955.
- [12] R. Han, A. Uneri, T. D. Silva, M. Ketcha, J. Goerres, S. Vogt, G. Kleinszig, G. Osgood, and J. H. Siewersden, "Atlas-based automatic planning and 3d-2d fluoroscopic guidance in pelvic trauma surgery," *Physics in Medicine & Biology*, vol. 64, p. 095022, May 2019.
- [13] P. Romero, M. Lozano, F. Martínez-Gil, D. Serra, R. Sebastián, P. Lamata, and I. García-Fernández, "Clinically-driven virtual patient cohorts generation: An application to aorta," *Frontiers in Physiology*, vol. 12, Sept. 2021.
- [14] X. yan Chen, W. W. Lam, H. K. Ng, Y. hua Fan, and K. S. Wong, "The frequency and determinants of calcification in intracranial arteries in chinese patients who underwent computed tomography examinations," *Cerebrovascular Diseases*, vol. 21, no. 1-2, pp. 91–97, 2006.
- [15] J. W. Bartstra, T. C. van den Beukel, W. V. Hecke, W. P. Mali, W. Spiering, H. L. Koek, J. Hendrikse, P. A. de Jong, and A. M. den Harder, "Intracranial arterial calcification: Prevalence, risk factors, and consequences," *Journal of the American College of Cardiology*, vol. 76, pp. 1595–1604, Sept. 2020.
- [16] M. S. M. Jones J, Murphy A, "Posterior communicating artery," 2009.
- [17] R. Bhalodia, S. Y. Elhabian, L. Kavan, and R. T. Whitaker, "DeepSSM: A deep learning framework for statistical shape modeling from raw images," in *Shape in Medical Imaging*, pp. 244–257, Springer International Publishing, 2018.

APPENDIX

A. Results of SSM for right ICA

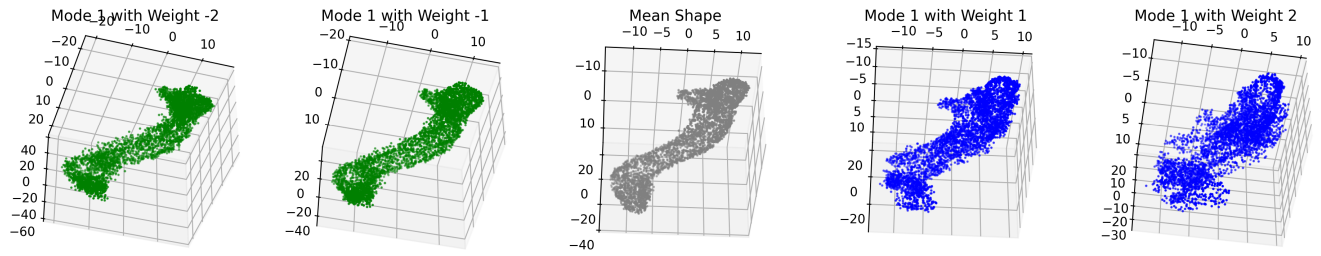


Figure 20: Mode 1 of the right ICA

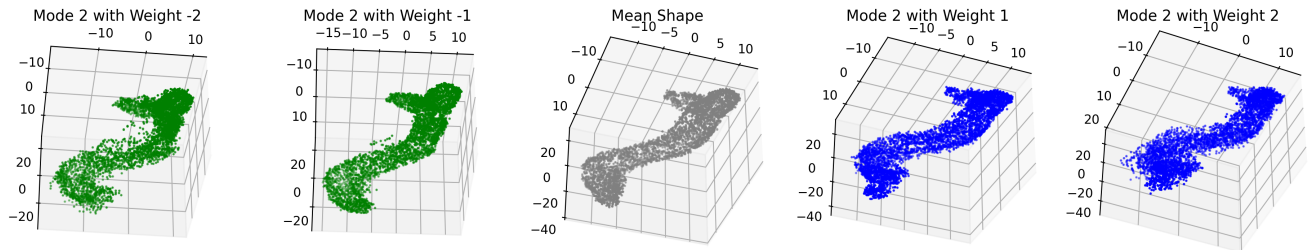


Figure 21: Mode 2 of the right ICA

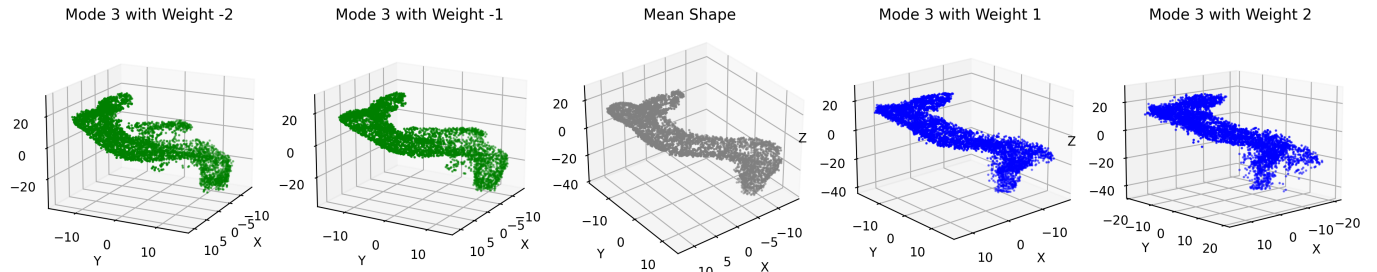


Figure 22: Mode 3 of the right ICA

The first three modes describe most of the shapes, so these are plotted to exemplify their effect.

We can see that mode 1 describes the diameter of the right ICA while mode 2 describes its curvature and it is unclear what mode 3 describes.

B. Results of SSM for left ICA

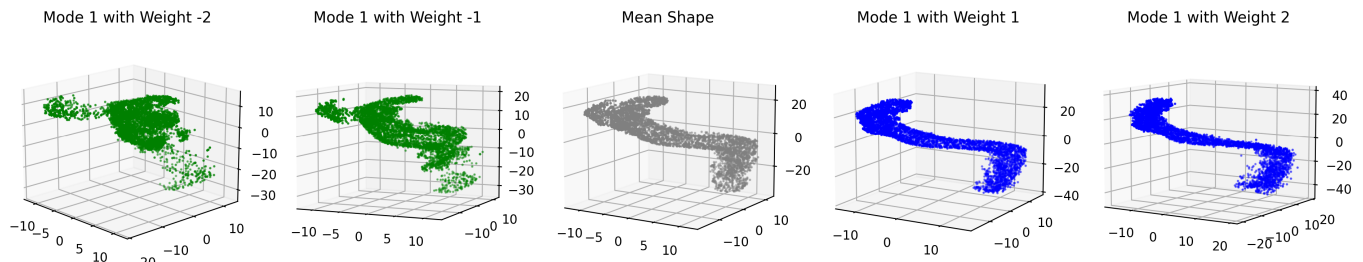


Figure 23: Mode 1 of the left ICA

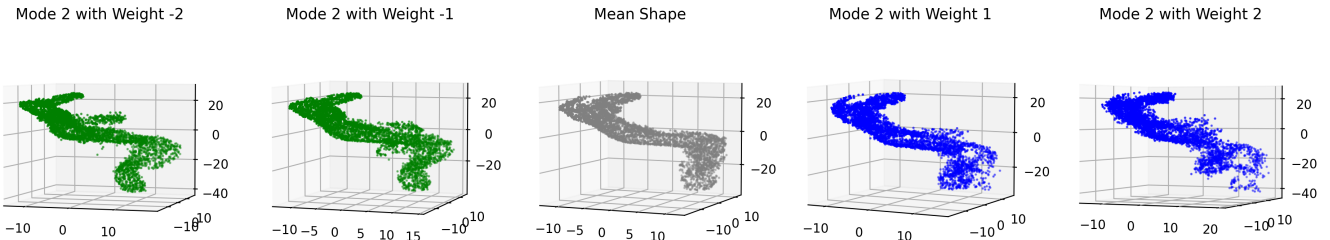


Figure 24: Mode 2 of the left ICA

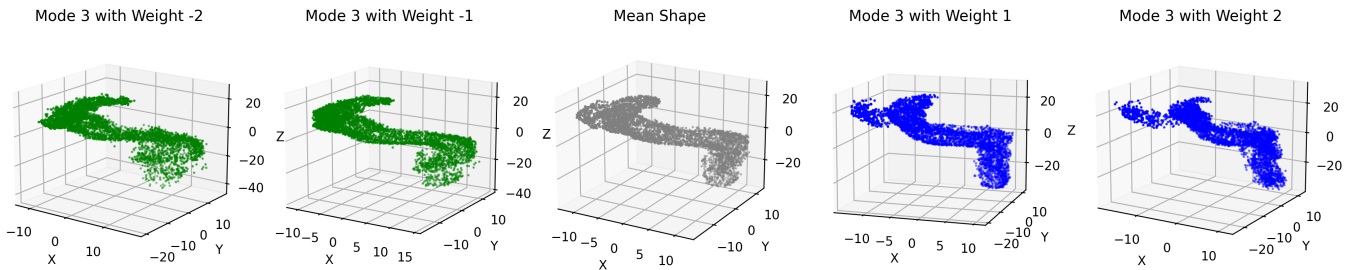


Figure 25: Mode 3 of the left ICA

The first three modes describe most of the shapes, so these are plotted to see their effect.

In the case of the Left ICA's, mode 1 seems to describe the overall volume and variation thereof, varying between short and large and long and thin. The second mode seems to vary the diameter/curvature of the bottom part (rightmost part in figure) of the left ICA. The third mode varies the overall diameter of the whole ICA.

C. Results of SSM vertebral artery

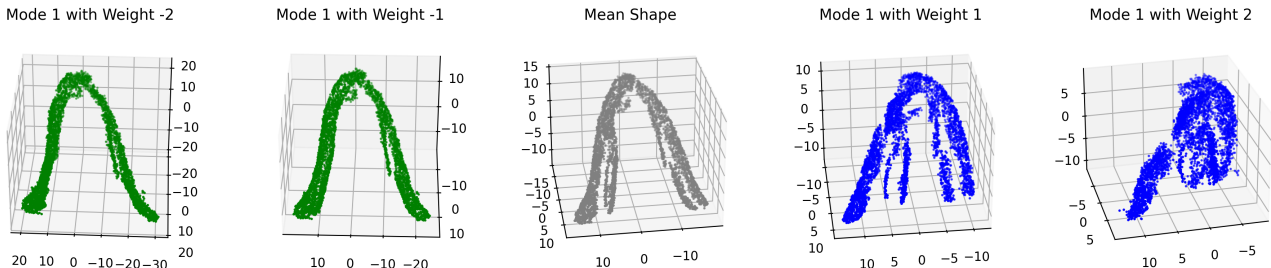


Figure 26: Mode 1 of the vertebral artery

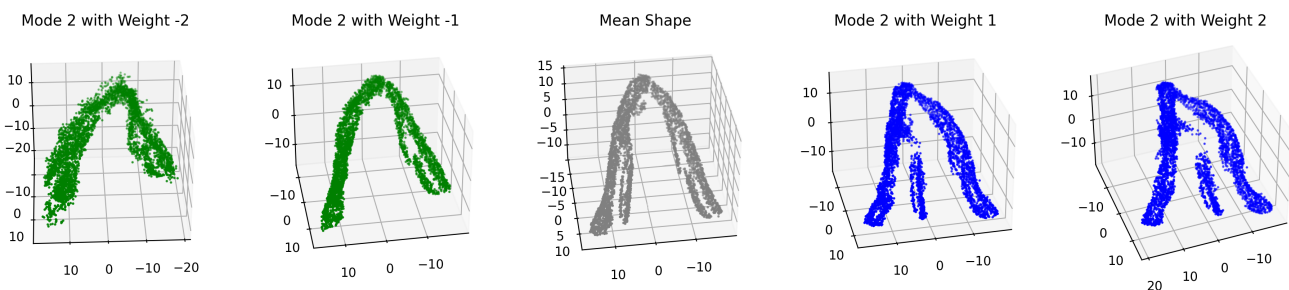


Figure 27: Mode 2 of the vertebral artery

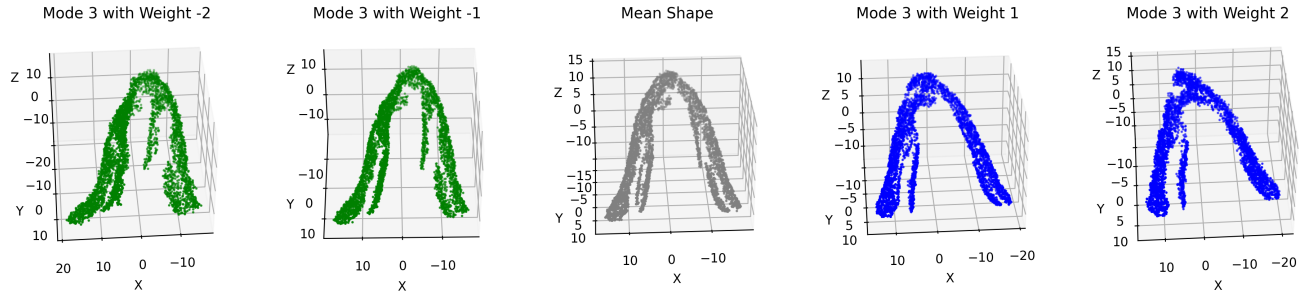


Figure 28: Mode 3 of the vertebral artery

The first three modes describe most of the shapes, so these are plotted to see their effect.

Mode 1 of the vertebral artery varies the diameter between the shapes. Mode 2 seems to mostly vary the length and curvature of the right part of the vertebral artery and Mode 3 varies the bifurcation angle

D. Results of SSM on basilar and posterior cerebral arteries

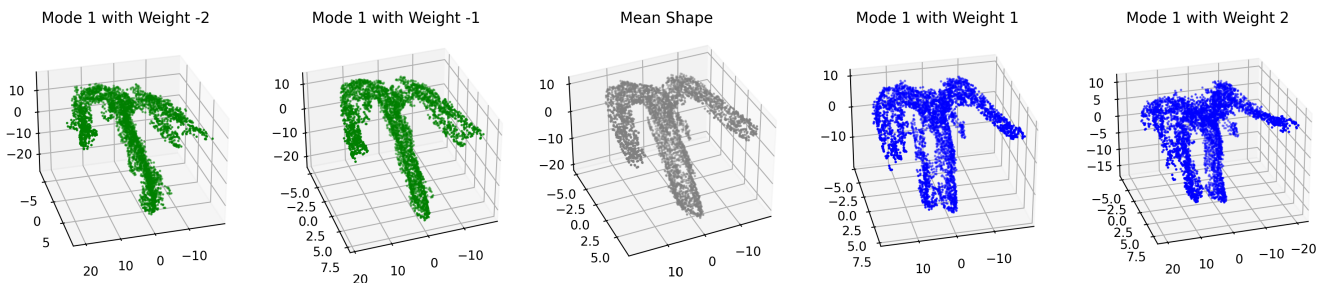


Figure 29: Mode 1 of the basilar and posterior cerebral arteries

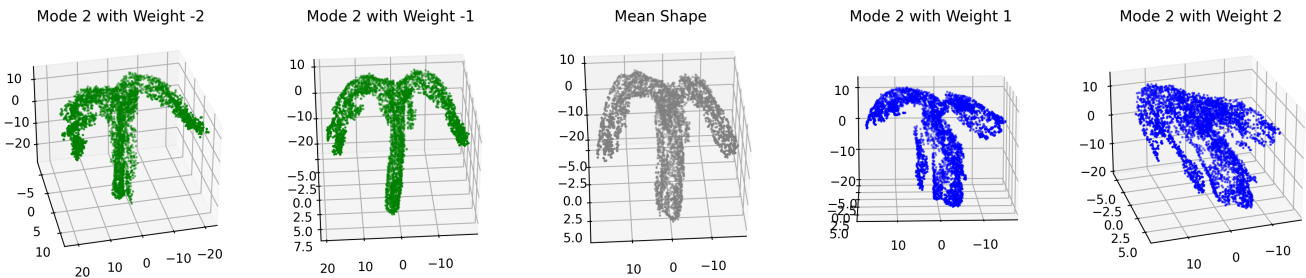


Figure 30: Mode 2 of the basilar and posterior cerebral arteries

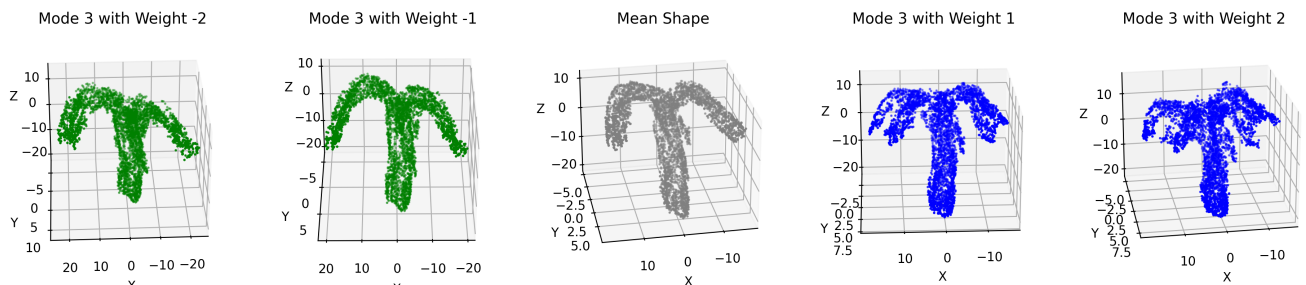


Figure 31: Mode 3 of the basilar and posterior cerebral arteries

The first three modes describe most of the shapes, so these are plotted to see their effect.

For the basilar and posterior cerebral arteries, mode 1 seems to induce a diameter variation which also seems the case for mode 2. Mode 3 however varies the curvature/ angle of the posterior cerebral arteries (the two branching arteries in the figures).

E. Results SSM on anterior cerebral arteries

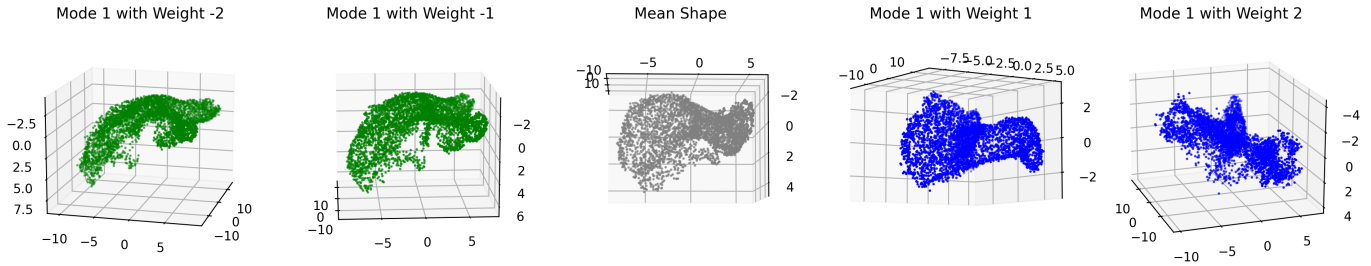


Figure 32: Mode 1 of the anterior communicating arteries

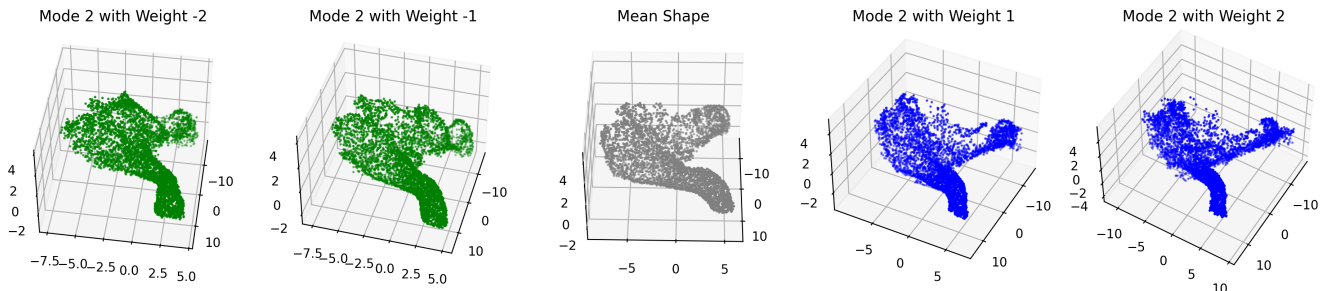


Figure 33: Mode 2 of the anterior communicating arteries

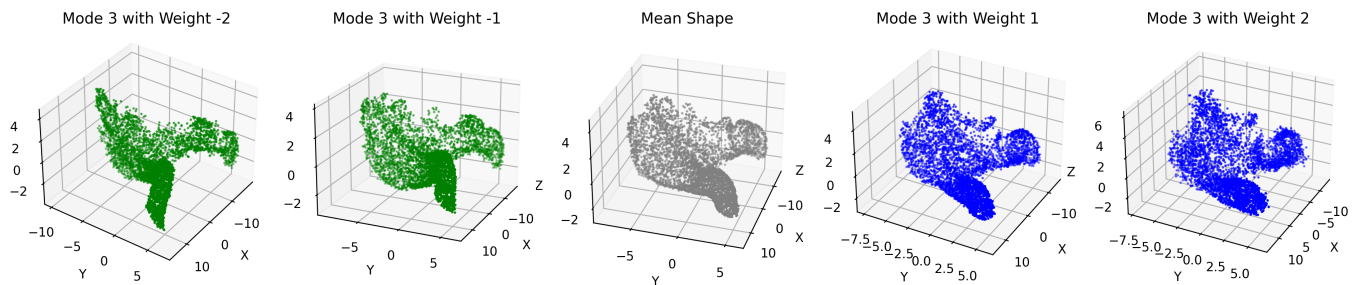


Figure 34: Mode 3 of the anterior communicating arteries

The first three modes describe most of the shapes, so these are plotted to see their effect.

Mode 1 of the anterior cerebral arteries varies the diameter, mode 2 varies the diameter and the angle of the communicating arteries. Mode 3 varies the curvature between the different weights .

F. p-value test

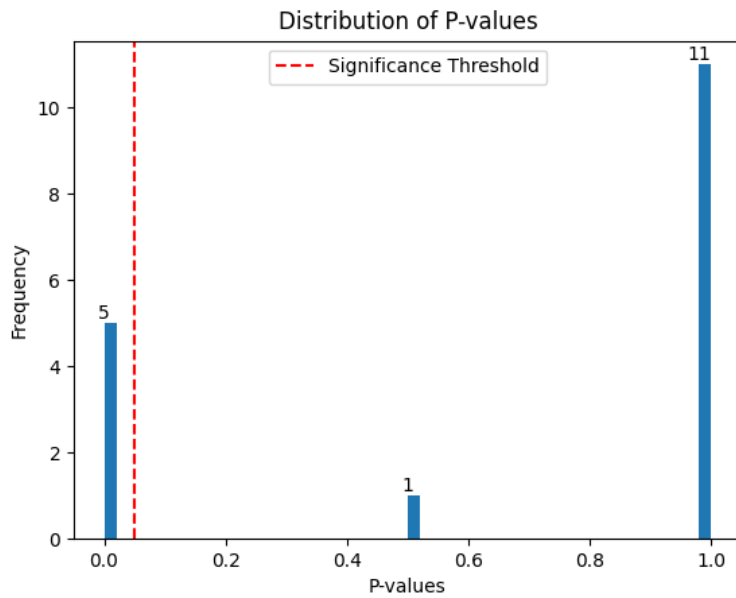


Figure 35: p-value test for right ICA

1) *Right ICA p-value test:* The p-value test takes an input shape, in this case the right ICA and indicates with a number between 0 and 1 how likely a specific mode of variability describes this shape. If the p-value is lower than 0.05 then the mode does contribute significantly to describing the specific object. In this case we can see that 5 modes contribute to the object whereas 1 has insignificant contribution and 11 do not contribute.

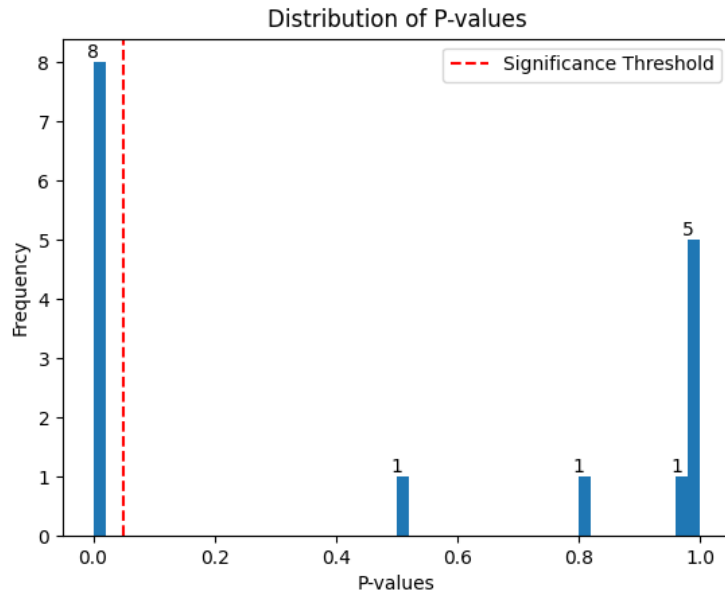


Figure 36: p-value test for left ICA

2) *Left ICA p-value test:* For a shape of the Left ICA, 8 modes describe this shape, 3 are insignificantly contributing and 5 do not contribute to the input shape.

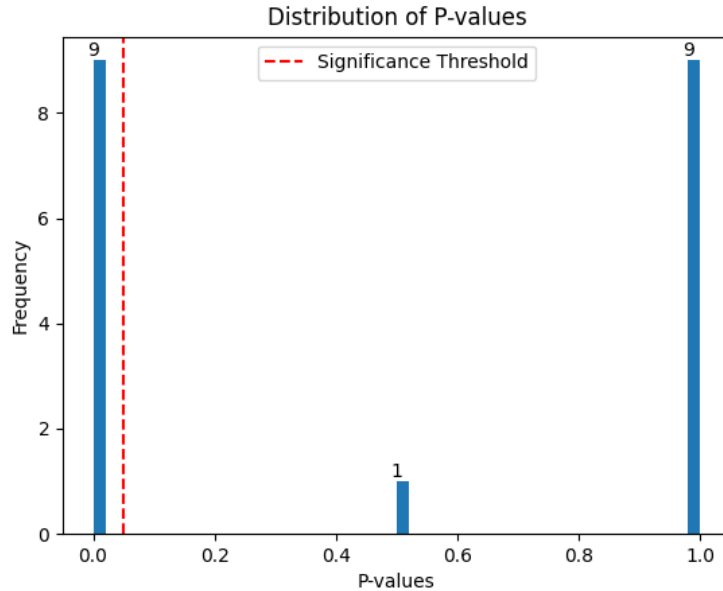


Figure 37: p-value test for basilar and posterior cerebral arteries

3) *Basilar and posterior cerebral arteries p-value test:* For a geometry of the basilar and posterior cerebral arteries, 9 modes describe this shape, 1 are statistically insignificant contributing and 9 do not contribute to the input shape.

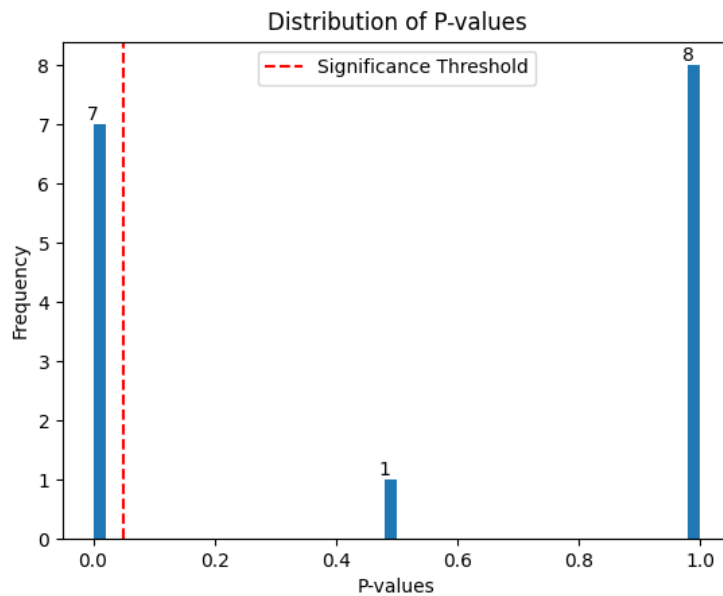


Figure 38: p-value test for vertebral arteries

4) *Vertebral Arteries p-value test:* For a geometry of the vertebral arteries, 7 modes describe this shape, 1 are statistically insignificant contributing and 8 do not contribute to the input shape.

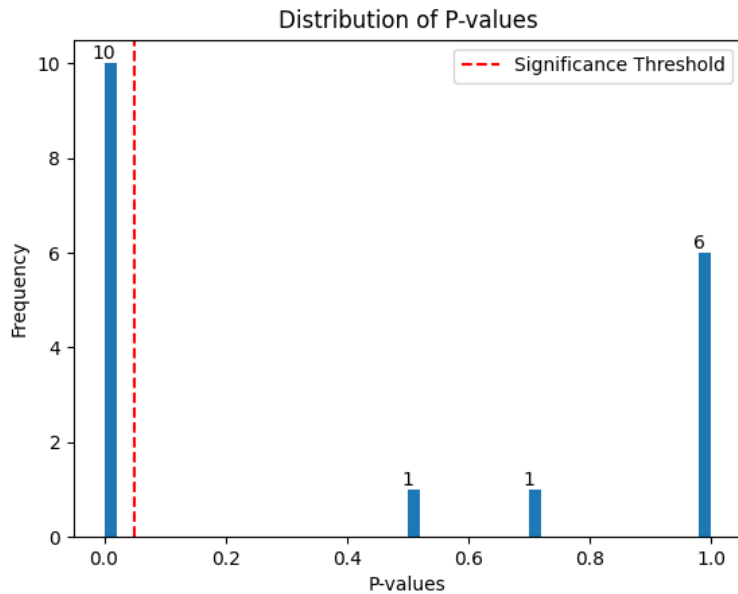


Figure 39: p-value test for anterior cerebral arteries

5) *Anterior cerebral arteries p-value test:* For a geometry of the Anterior cerebral arteries, 10 modes describe this shape, 2 are statistically insignificant contributing and 6 do not contribute to the input shape.

G. Link to the GitHub

The link to the GitHub is below. All the code is made available there as well as the STL files used in the study.
https://github.com/noahsaad10/SSM_BEP.git